Supplementary Information

Nondestructive halide exchange via S_N2-like mechanism for efficient blue perovskite light-emitting diodes

Kai Zhang[1,†], Yang Shen[1,2,†,*], Long-Xue Cao[2,†], Zhen-Huang Su[3], Xin-Mei Hu[2], Shi-Chi Feng[2], Bing-Feng Wang[4], Feng-Ming Xie[2], Hao-Ze Li[4], Xingyu Gao[3], Yan-Qing Li[4,*], and Jian-Xin Tang[1,2,*]

[1] Macao Institute of Materials Science and Engineering (MIMSE), Faculty of Innovation Engineering
Macau University of Science and Technology
Taipa 999078, Macao, China

[2] Institute of Functional Nano & Soft Materials (FUNSOM), Jiangsu Key Laboratory for Carbon-Based Functional Materials & Devices
Soochow University
Suzhou 215123, China

[3] Shanghai Synchrotron Radiation Facility
Zhangjiang Laboratory, Chinese Academy of Sciences
Shanghai 200241, China

[4] School of Physics and Electronic Science
East China Normal University
Shanghai 200241, China

[†] These authors contributed equally to this work.

* Corresponding author. Email address: jxtang@must.edu.mo (J.X. Tang), yangshen@suda.edu.cn (Y. Shen), yqli@phy.ecnu.edu.cn (Y.Q. Li)

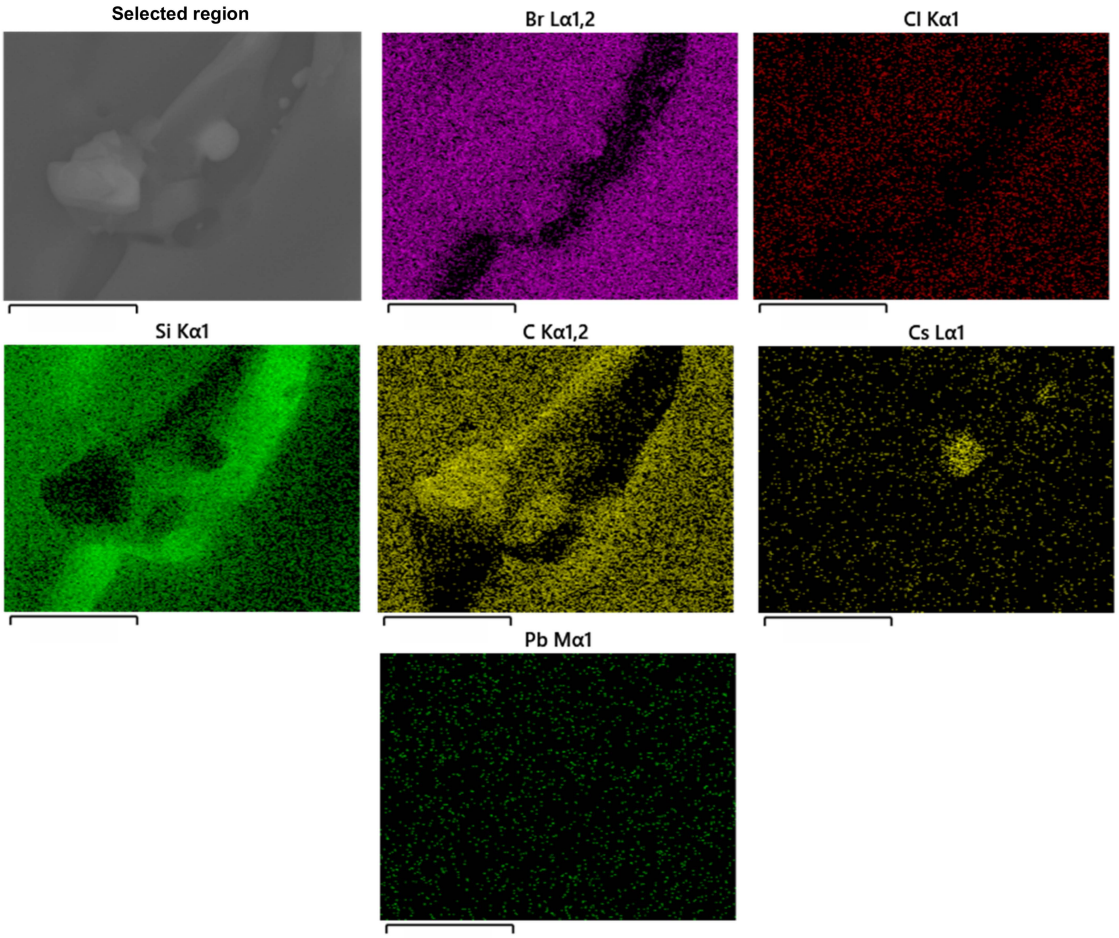

Supplementary Fig. 1. Element distribution of the IPA stripped sample. EDS mapping of the element components stripped from the perovskite films by IPA solvent post-treatment. Scale bars: 5 μm.

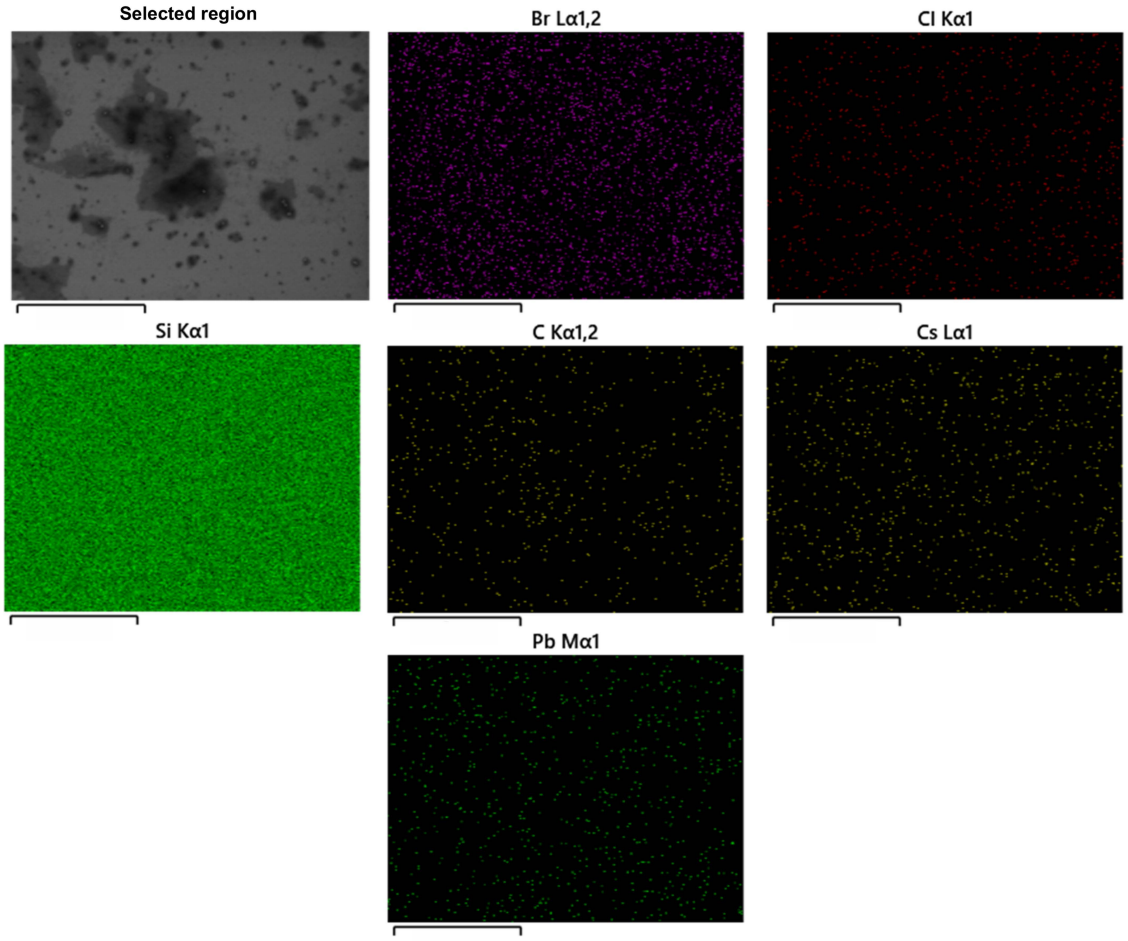

Supplementary Fig. 2. Element distribution of the CF stripped sample. EDS mapping of the element components stripped from the perovskite films by CF solvent post-treatment. Scale bars: 5 μm.

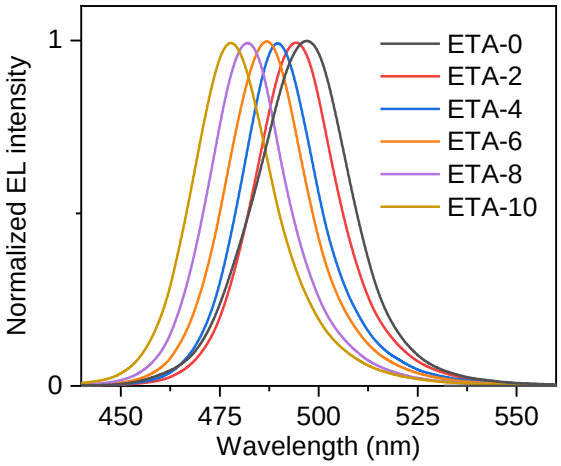

Supplementary Fig. 3. EL spectral evolution with ETA ratios. Normalized EL spectra of PeLEDs based on HTL layers with different ETA doping ratios (0, 2, 4, 6, 8, 10 vol. ‰).

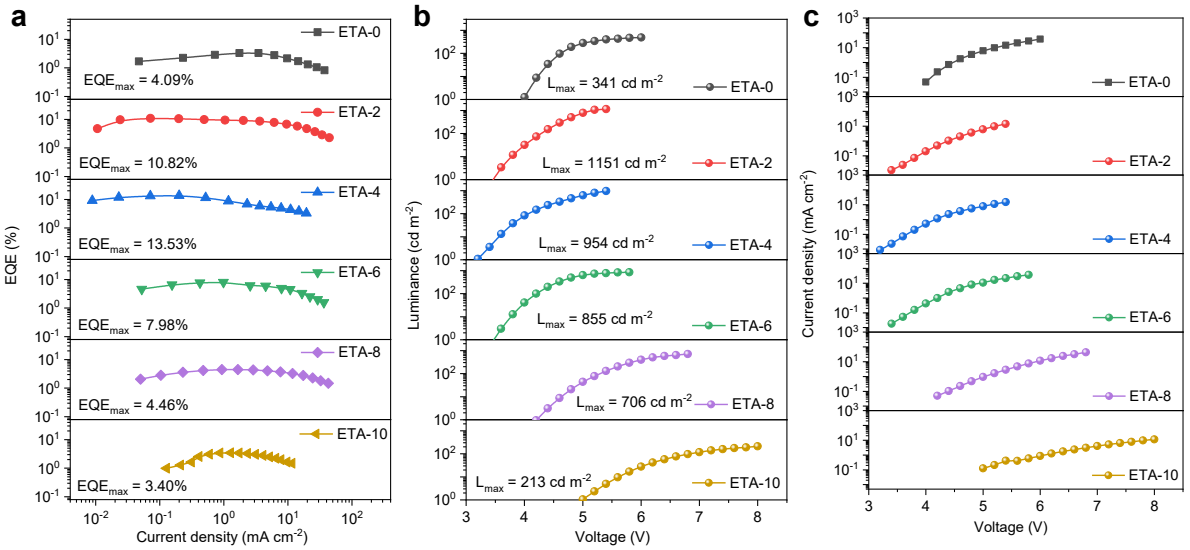

Supplementary Fig. 4. EL characteristics of PeLEDs with different ETA doping ratios (0-10 vol.%). **a** Dependence of the EQE versus current density. **b** Luminance-voltage (*L*-*V*) characteristics. **c** Current density-voltage (*J*-*V*) characteristics.

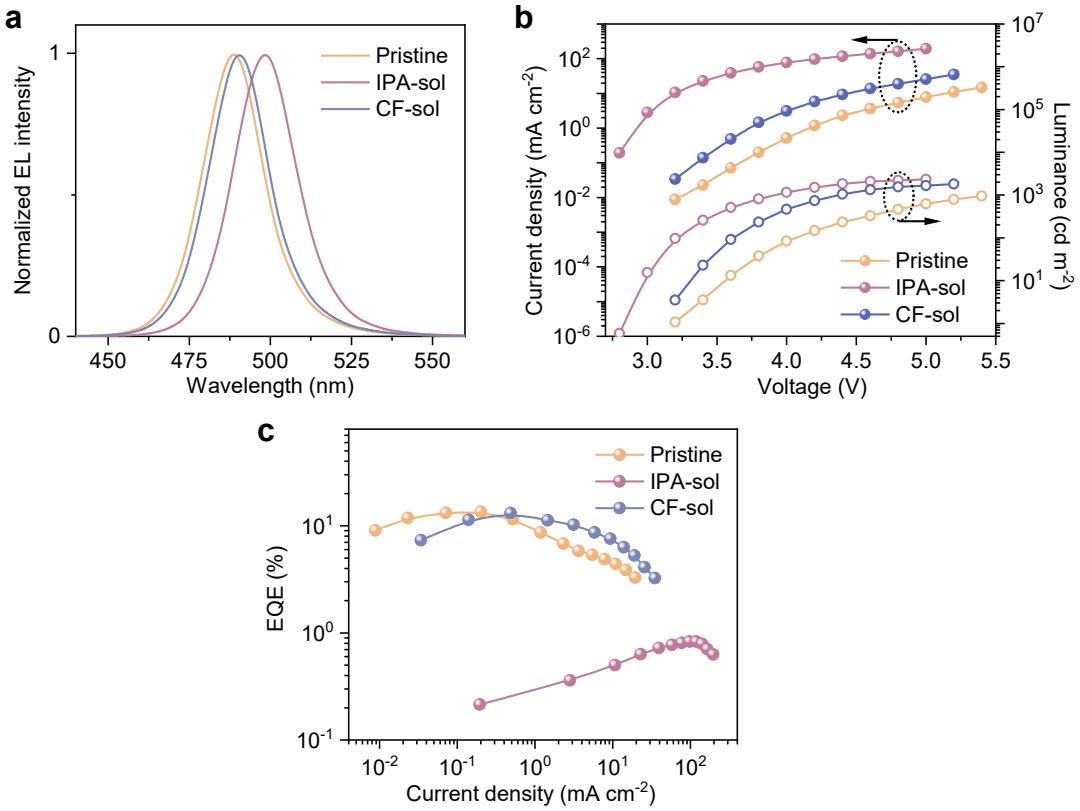

Supplementary Fig. 5. EL characteristics of pristine and solvent post-treated PeLEDs. a Normalized EL spectra. **b** *J-V-L* characteristic curves. **c** EQE curves based on pristine and different solvent post-processed devices. The distinct device *J-V-L* characteristics can be ascribed to the stripping effect of IPA and CF. Although CF can hardly dissolve perovskites, it can remove the excess $PbBr_2$ particles due to mechanical solvent scour, thereby impacting the interfacial charge transport.

Supplementary Fig. 6. Solubility of ligands for post-treatment. Photographs of BABr (left) and *p*-F-PEABr (right) in CF (5 mg mL^{-1}).

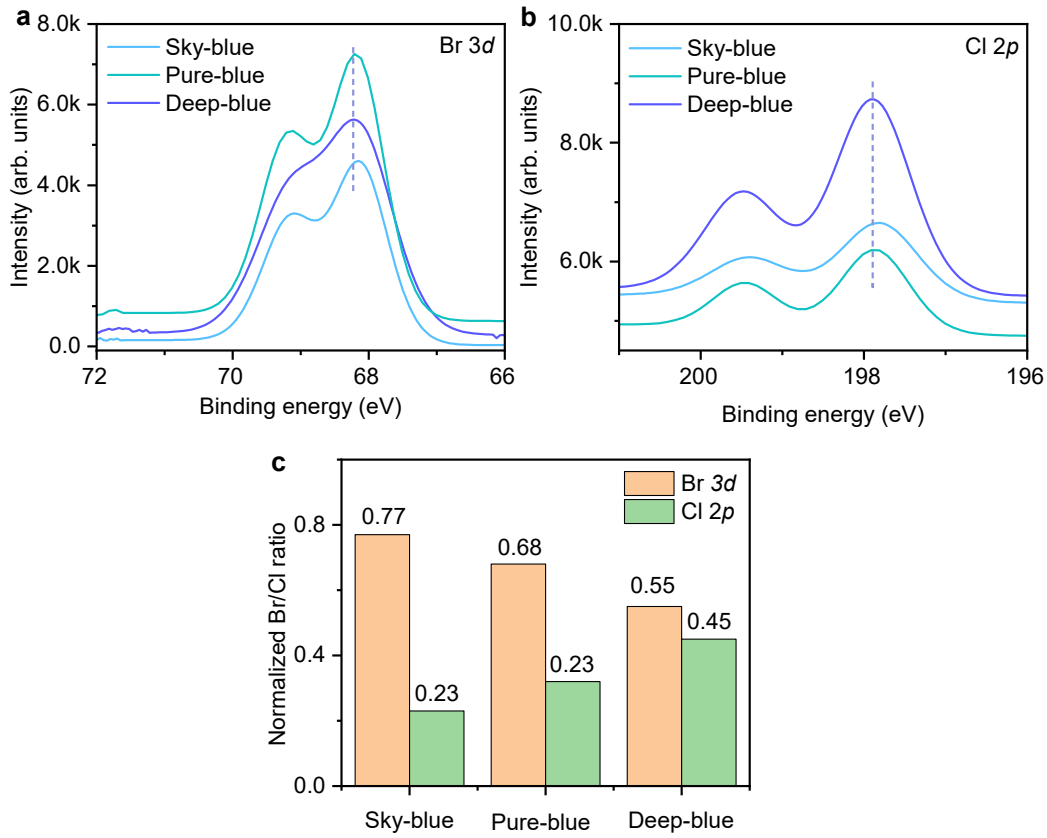

Supplementary Fig. 7. Halogen ratios in blue perovskite films. a, b XPS spectra of (**a**) Br 3*d* and (**b**) Cl 2*p* from the perovskite films with BACl/BABr solution post-treatment. The inconsistency in the trend of peak intensities arises from variations in signal strength during testing. **c** Normalized Br/Cl ratios in the perovskite films with BACl/BABr solution post-treatment. The detailed process for calculating the absolute content of halogen atoms is provided in Supplementary Table 2.

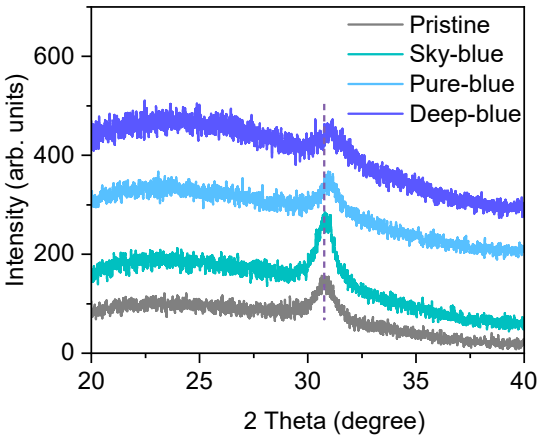

Supplementary Fig. 8. Perovskite crystalline evolution by CF post-treatment. Regular XRD patterns of pristine and CF post-treated perovskite films.

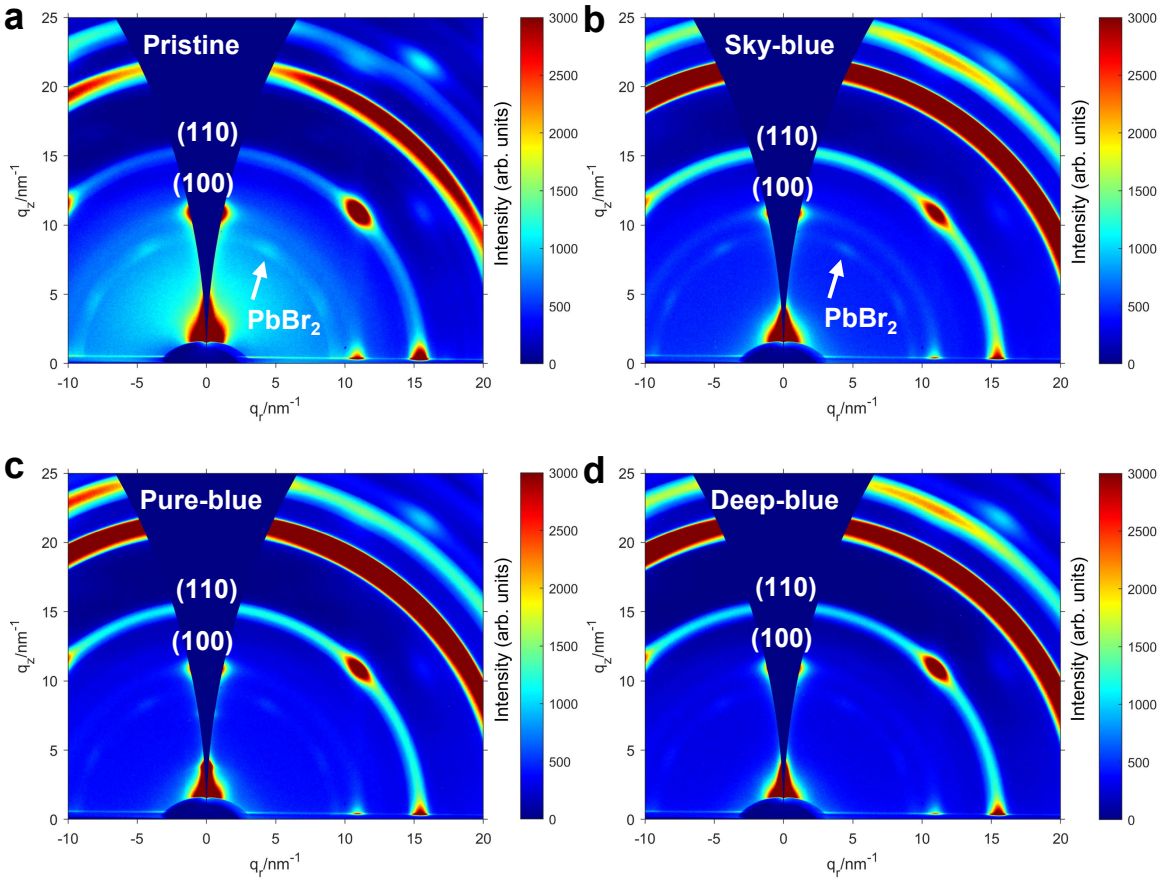

Supplementary Fig. 9. Crystalline information of perovskite films. GIWAXS patterns of the (**a**) pristine, (**b**) sky-, (**c**) pure-, and (**d**) deep-blue perovskite films.

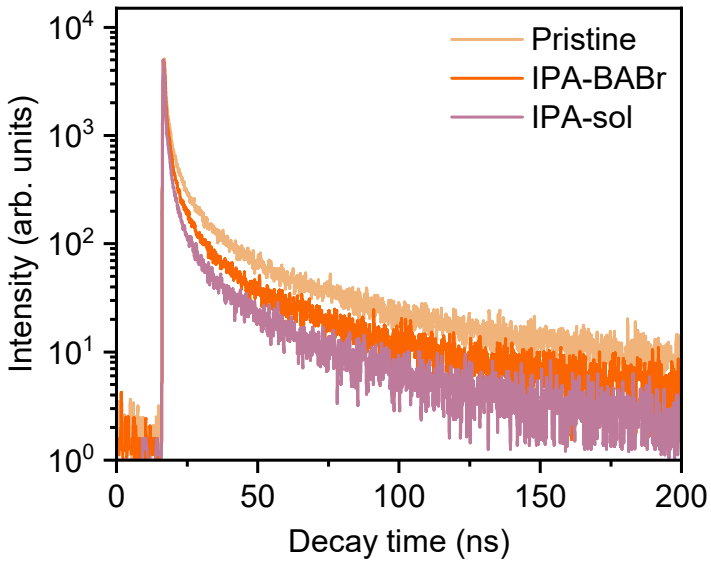

Supplementary Fig. 10. Influence of IPA post-treatment on exciton dynamics. Time-resolved PL spectra of pristine, pure IPA, and BABr incorporated IPA post-treated perovskite films.

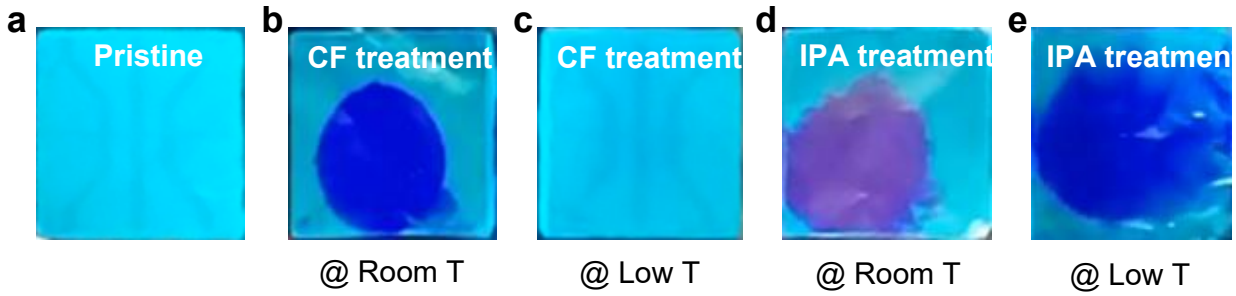

Supplementary Fig. 11. Photoluminescence images of perovskite films. **a** Pristine film. **b**, **c** BACl-incorporated CF post-treated films at (**b**) room and (**c**) low temperature. **d**, **e** BACl-incorporated IPA post-treated films at (**d**) room and (**e**) low temperature.

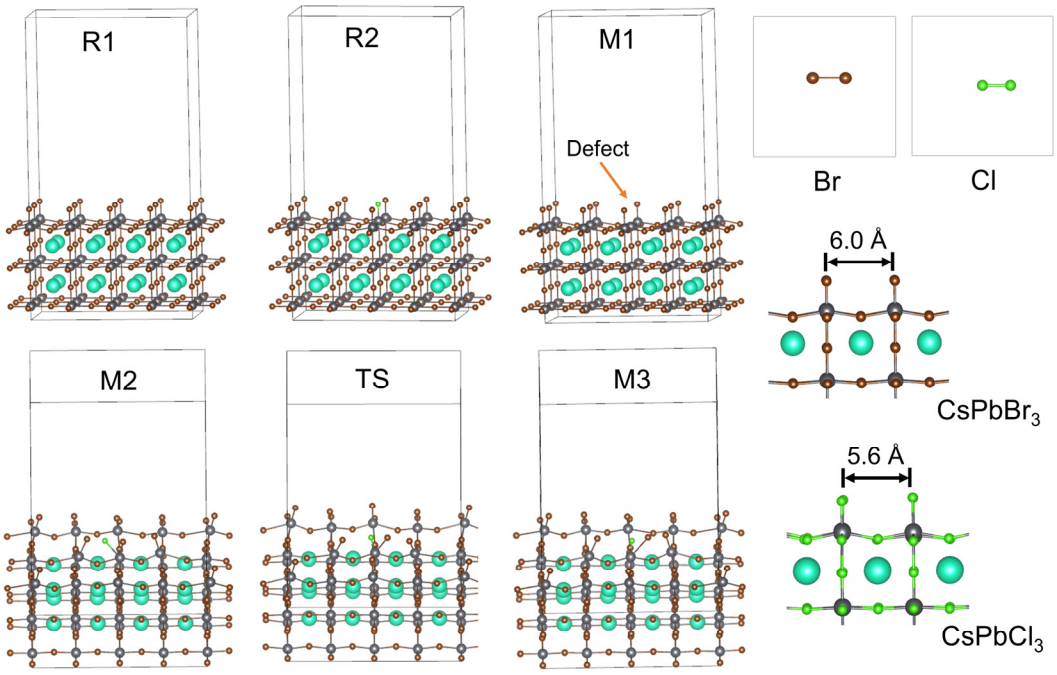

Supplementary Fig. 12. The crystal structures corresponding to different states in theoretical simulations. (R1: reactants, $CsPbBr_3$+Cl. R2: product, $CsPbBr_2Cl$ +Br. Intermediate for S_N1-like process: M1: surface defects of Br, $CsPbBr_2$-defect +Br+Cl. Intermediate for S_N2-like process: M2: Cl adsorbed in crystal surface, $CsPbBr_3$•••Cl; M3: Br adsorbed in crystal surface, $CsPbBr_2Cl$•••Br; TS1: transition states, $CsPbBr_2$•••Br•••Cl.)

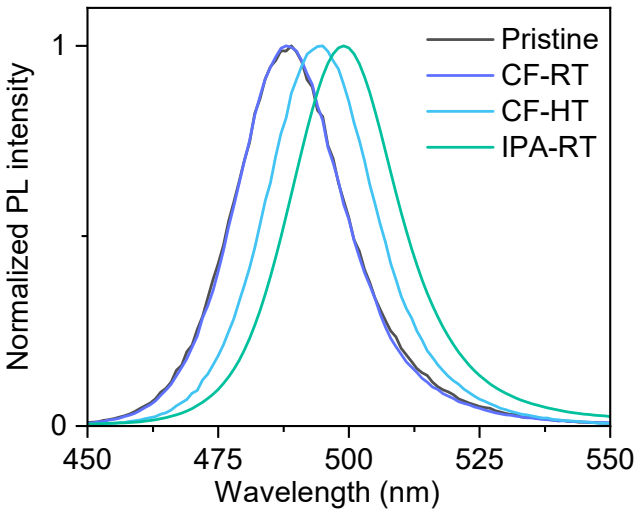

Supplementary Fig. 13. PL spectra of pristine and BABr incorporated post-treatment perovskite films. RT represents the room temperature and HT represents the high temperature of substrate and solution at 60°C.

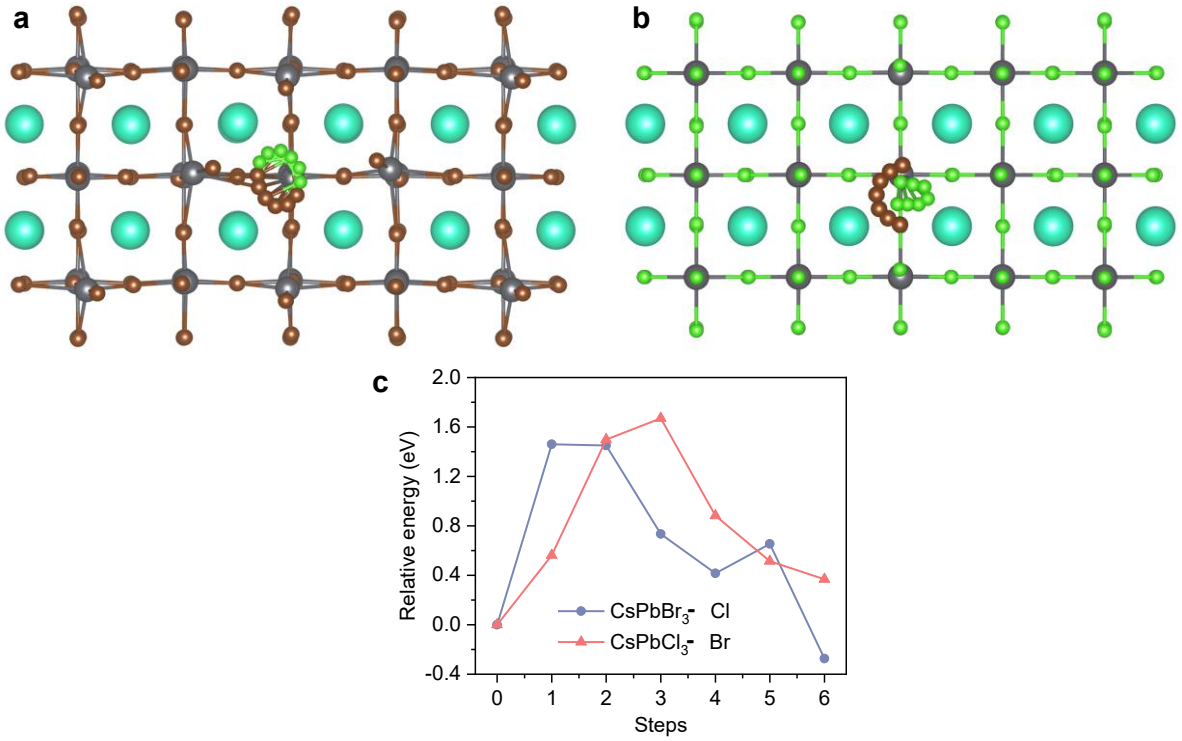

Supplementary Fig. 14. Theoretical modeling of the substitution of Br for Cl ions based on the S_N2-like mechanism. a, b Theoretical model of the ion exchange pathway for (**a**) Br substitution of Cl and (**b**) Cl substitution of Br in perovskite lattices. **c** Relative energy landscapes of the system during the ion exchange process. The x axis indicates the steps of exchange of spatial positions of halide atoms.

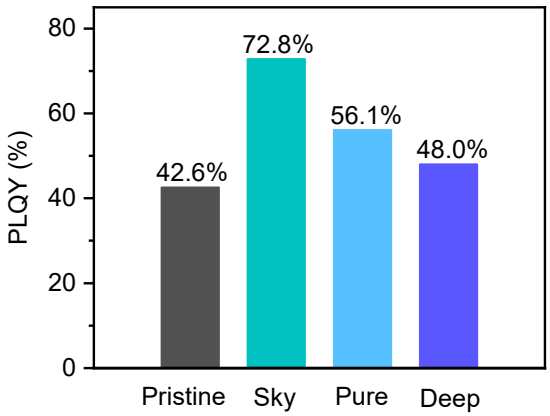

Supplementary Fig. 15. PLQYs of perovskite films. PLQYs of pristine perovskite film, and sky-, pure-, and deep-blue perovskite films by CF post-treatment.

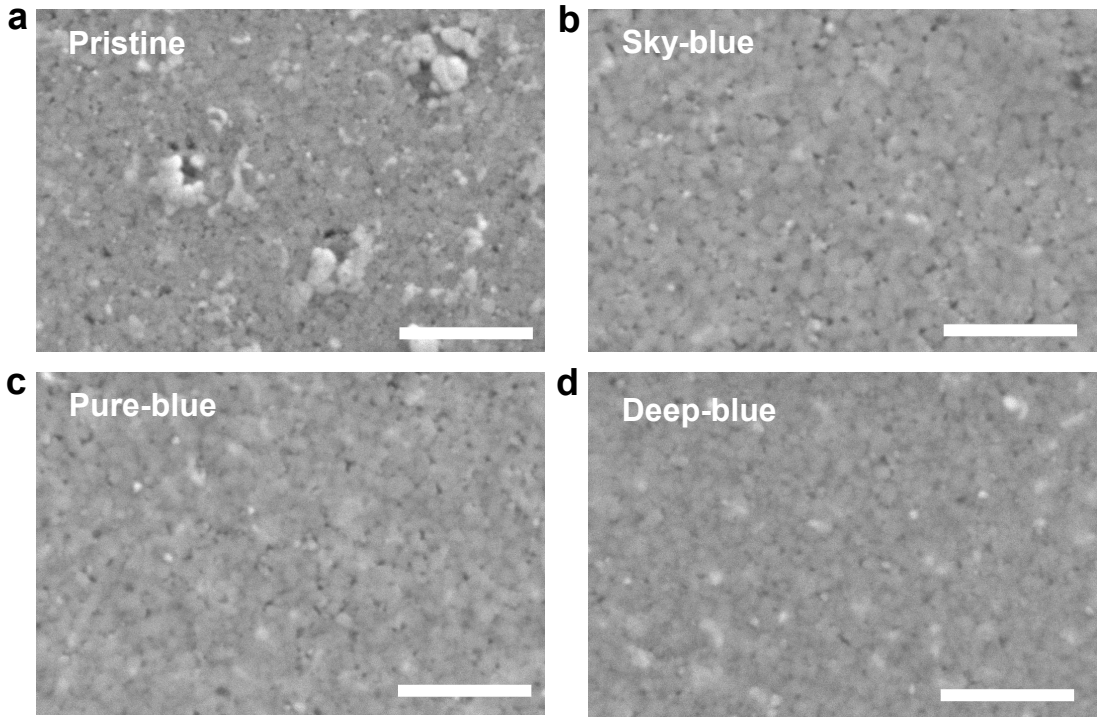

Supplementary Fig. 16. Morphological characterization of perovskite films. a-d Top-view SEM images of (**a**) pristine, (**b**) sky-, (**c**) pure-, and (**d**) deep-blue perovskite films with CF-based post-treatment. Scale bars: 300 nm.

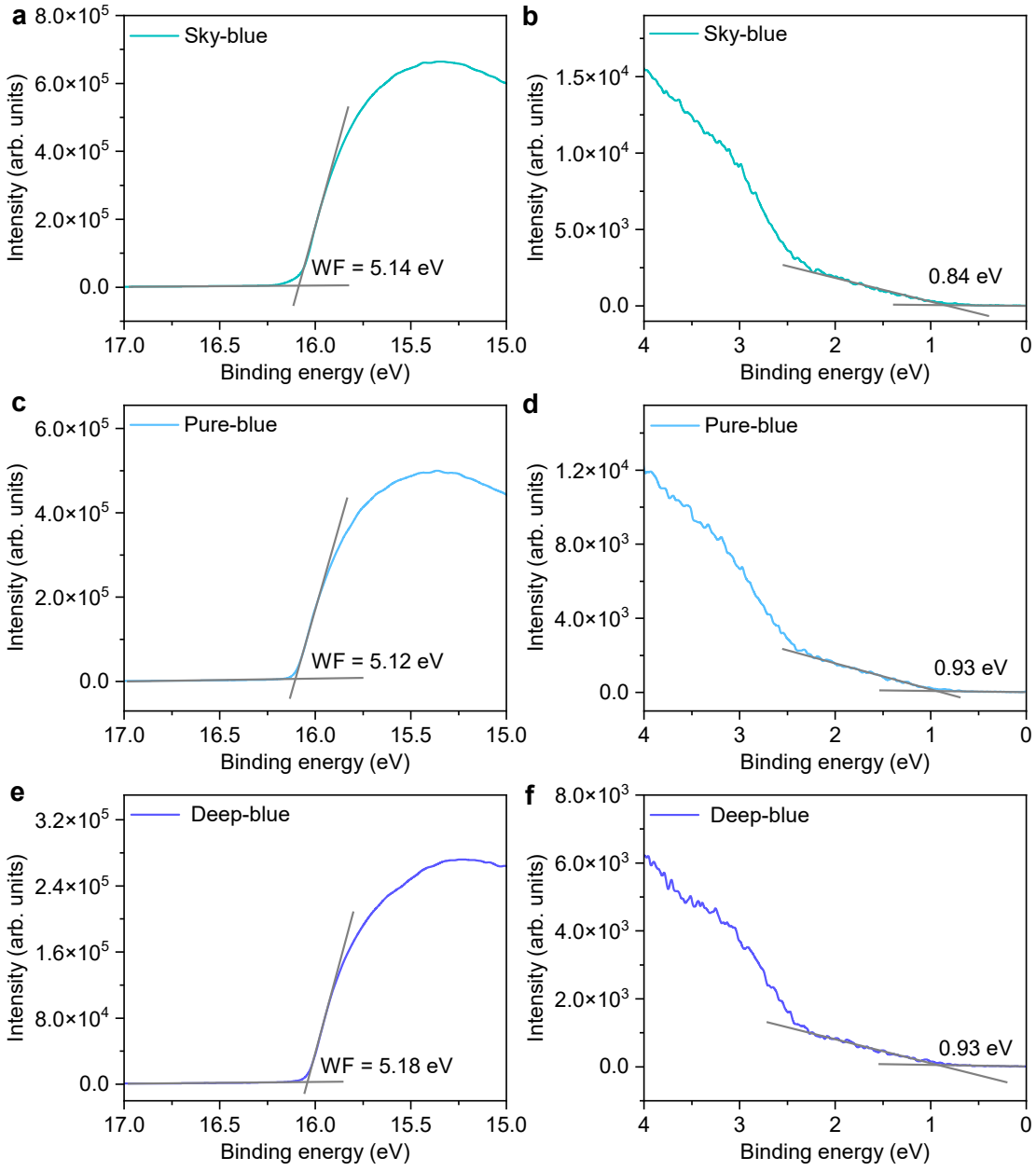

Supplementary Fig. 17. UPS measurements of perovskite films. a, c, e Secondary-electron cutoff regions in the UPS spectra of (**a**) sky-, (**c**) pure-, (**e**) and deep-blue perovskite films. **b, d, f** Secondary-electron onset regions of (**b**) sky-, (**d**) pure-, (**f**) and deep-blue perovskite films.

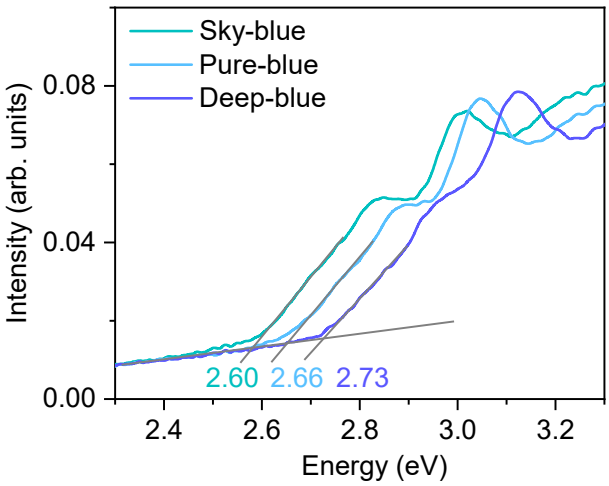

Supplementary Fig. 18. Optical band gaps of target perovskite films. Tauc plot analysis for the absorption spectra of CF post-treated perovskite films.

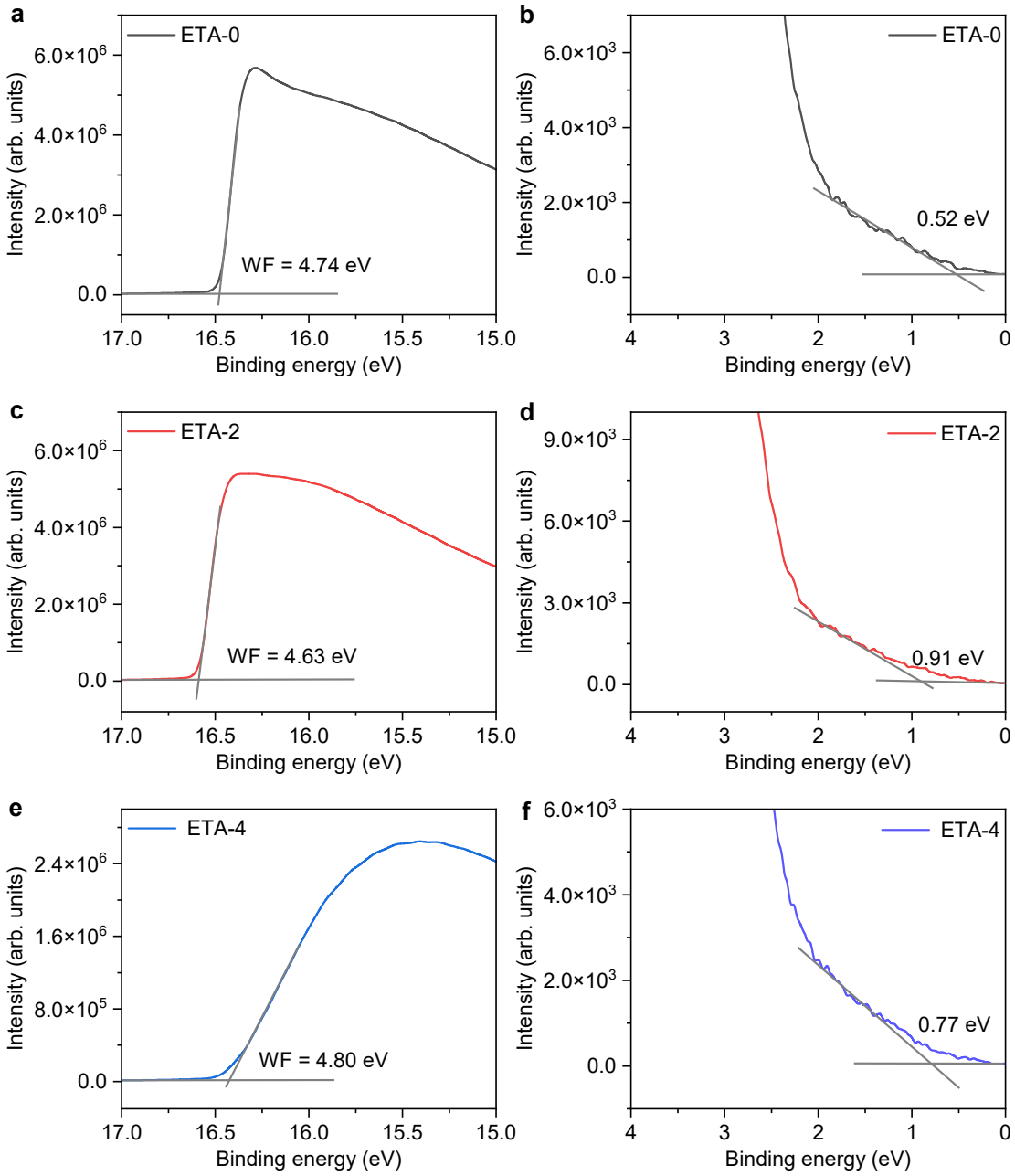

Supplementary Fig. 19. UPS measurements of ETA-modified PEDOT:PSS films. a, c, e Secondary-electron cutoff regions in the UPS spectra of (**a**) ETA-0 (pristine PEDOT:PSS), (**c**) ETA-2, (**e**) and ETA-4 films. **b, d, f** Secondary-electron onset regions of (**b**) ETA-0 (PEDOT:PSS), (**d**) ETA-2, (**f**) and ETA-4 films.

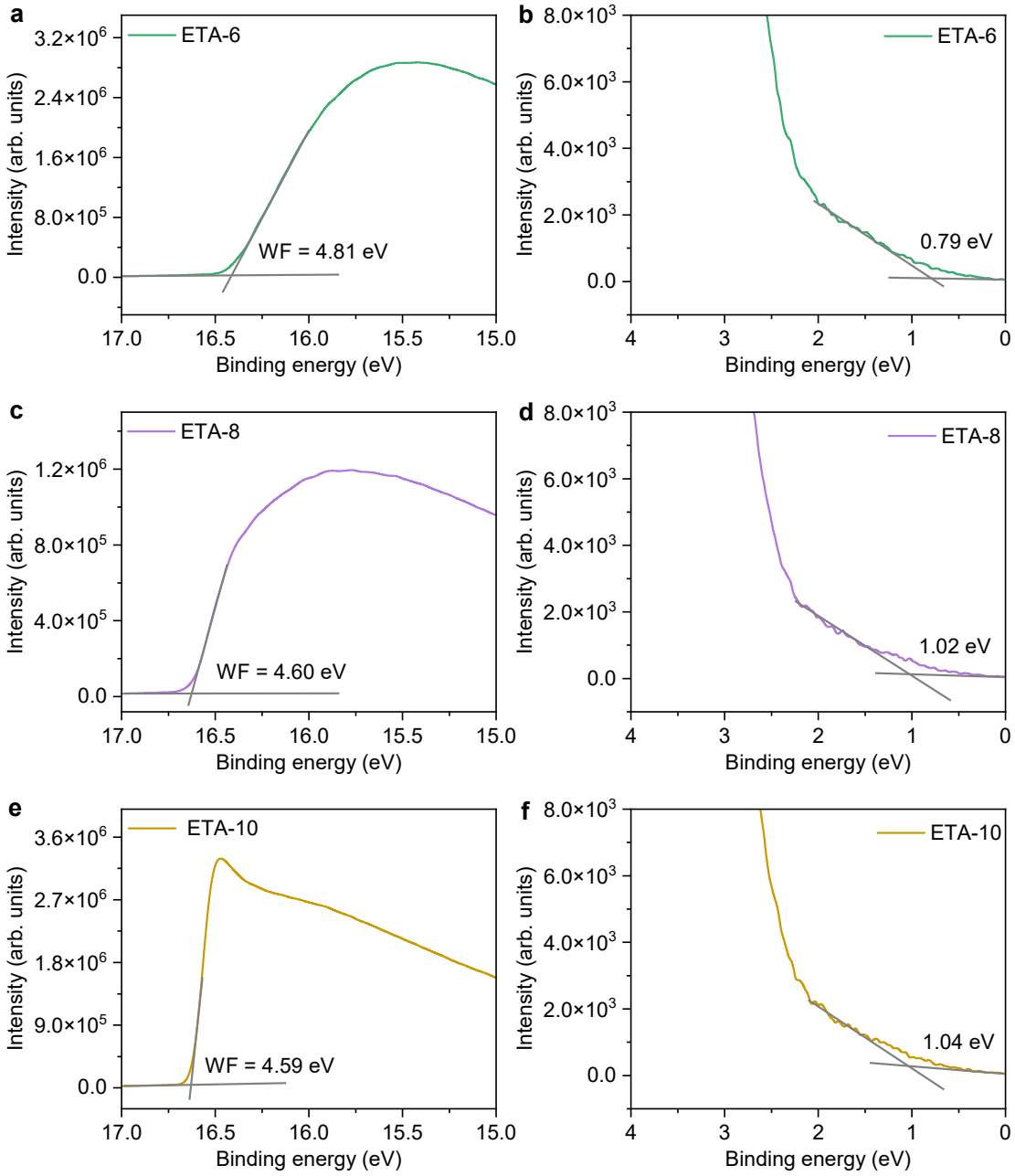

Supplementary Fig. 20. UPS measurements of ETA-modified PEDOT:PSS films. a, c, e Secondary-electron cutoff regions in the UPS spectra of (**a**) ETA-6, (**c**) ETA-8, (**e**) and ETA-10 films. **b, d, f** Secondary-electron onset regions of (**b**) ETA-6, (**d**) ETA-8, (**f**) and ETA-10 films.

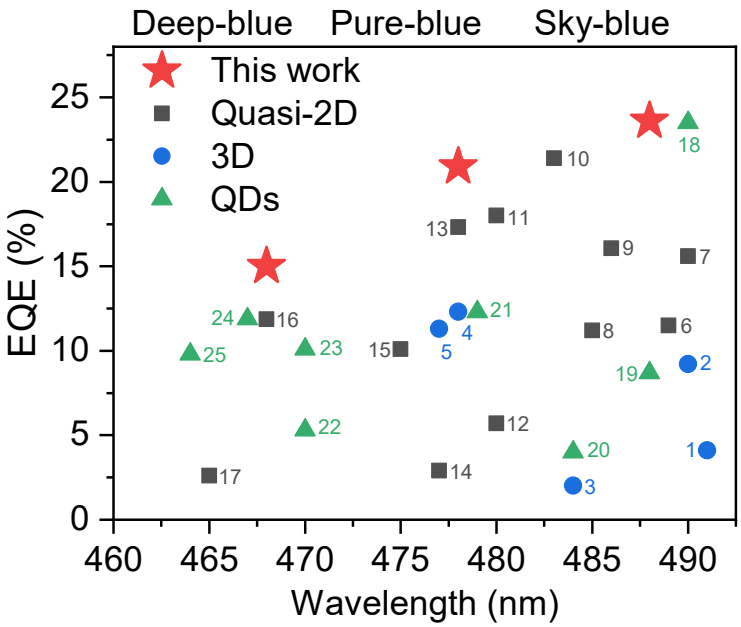

Supplementary Fig. 21. Performance evaluation of target blue PeLEDs. EQE statistics of the state-of-the-art PeLEDs from deep- to sky-blue spectral range.

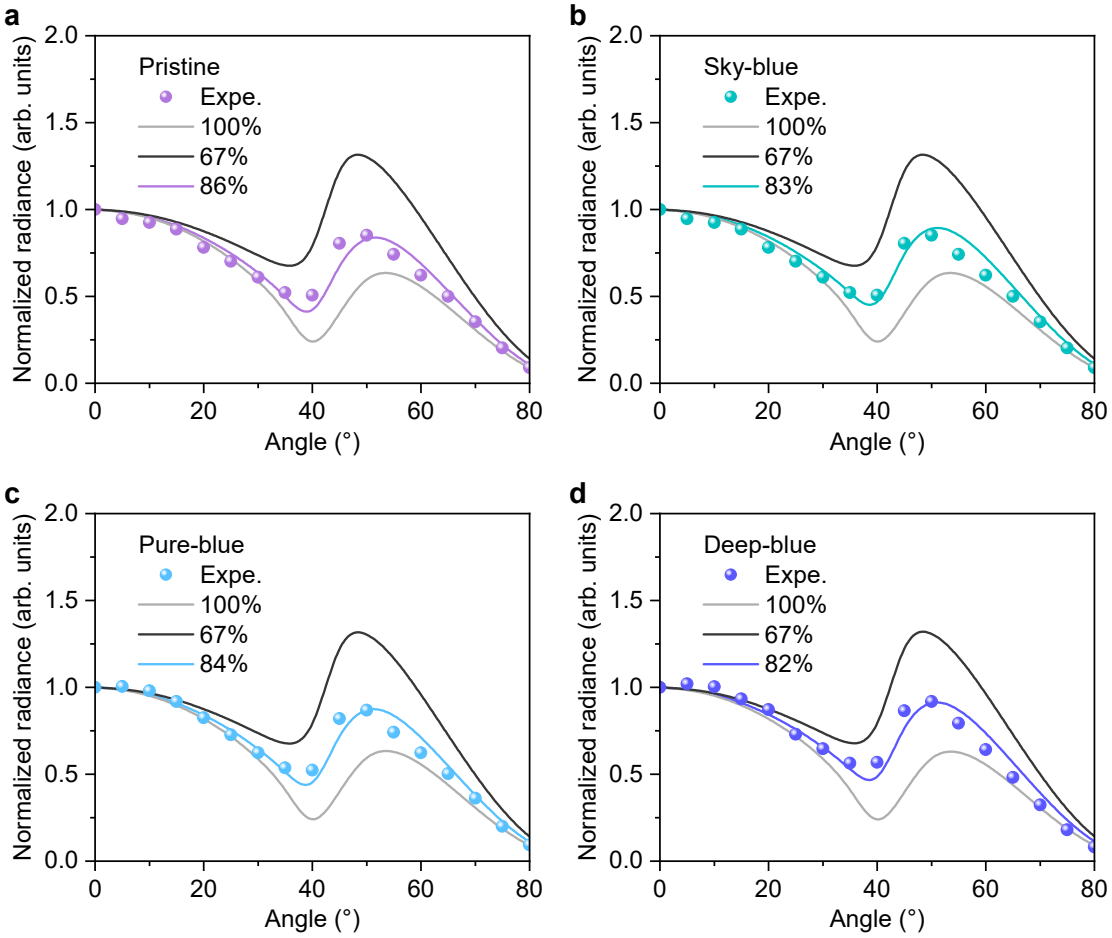

Supplementary Fig. 22. Horizontal transition dipole moments measurement of perovskite films. Angle-dependent PL measurements of (**a**) pristine (Θ: 86%), (**b**) sky-blue (Θ: 83%), (**c**) pure-blue (Θ: 84%), and (**d**) deep-blue (Θ: 82%) perovskite film. The orientation of TDMs in the qusai-2D film is quantified as the ratio of horizontal TDMs, denoted by Θ.

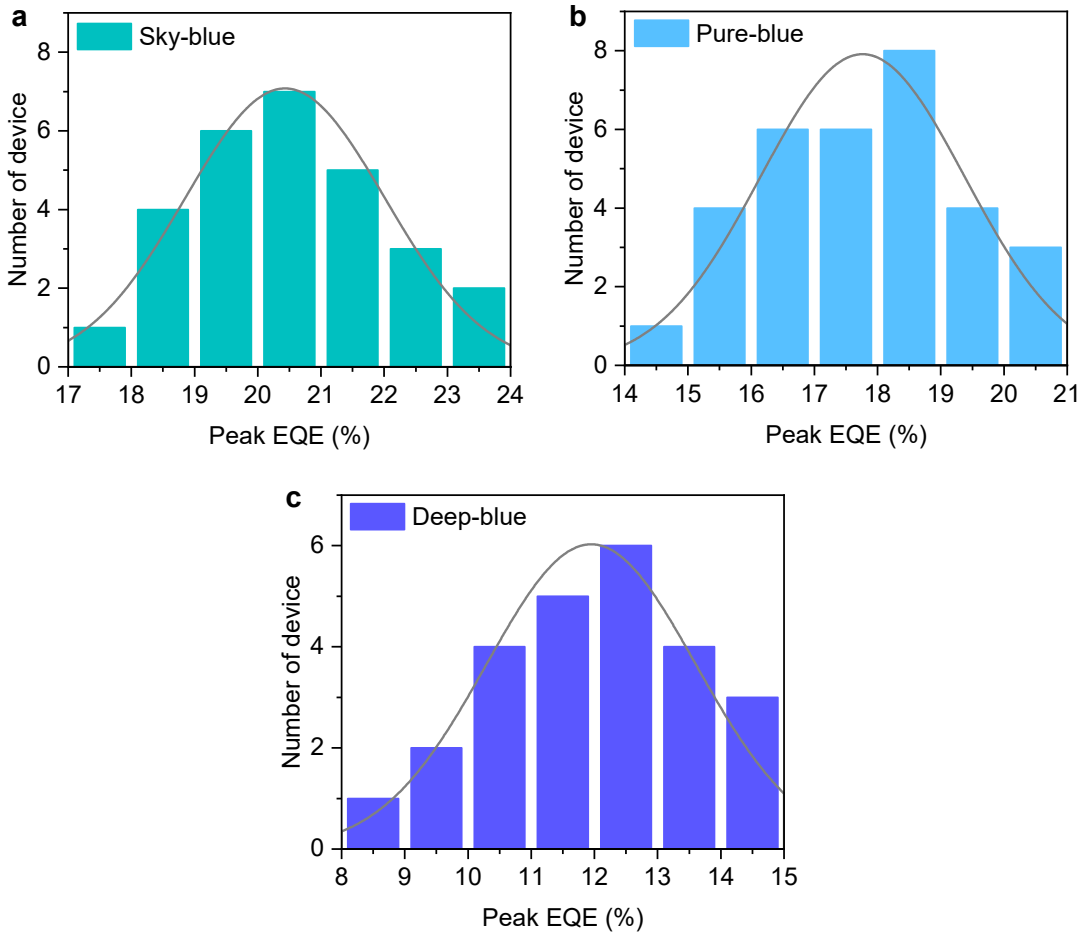

Supplementary Fig. 23. EQE statistics of CF post-treated devices. Statistical charts of the peak EQEs of (**a**) sky-, (**b**) pure-, and (**c**) deep-blue devices with CF post-treatment.

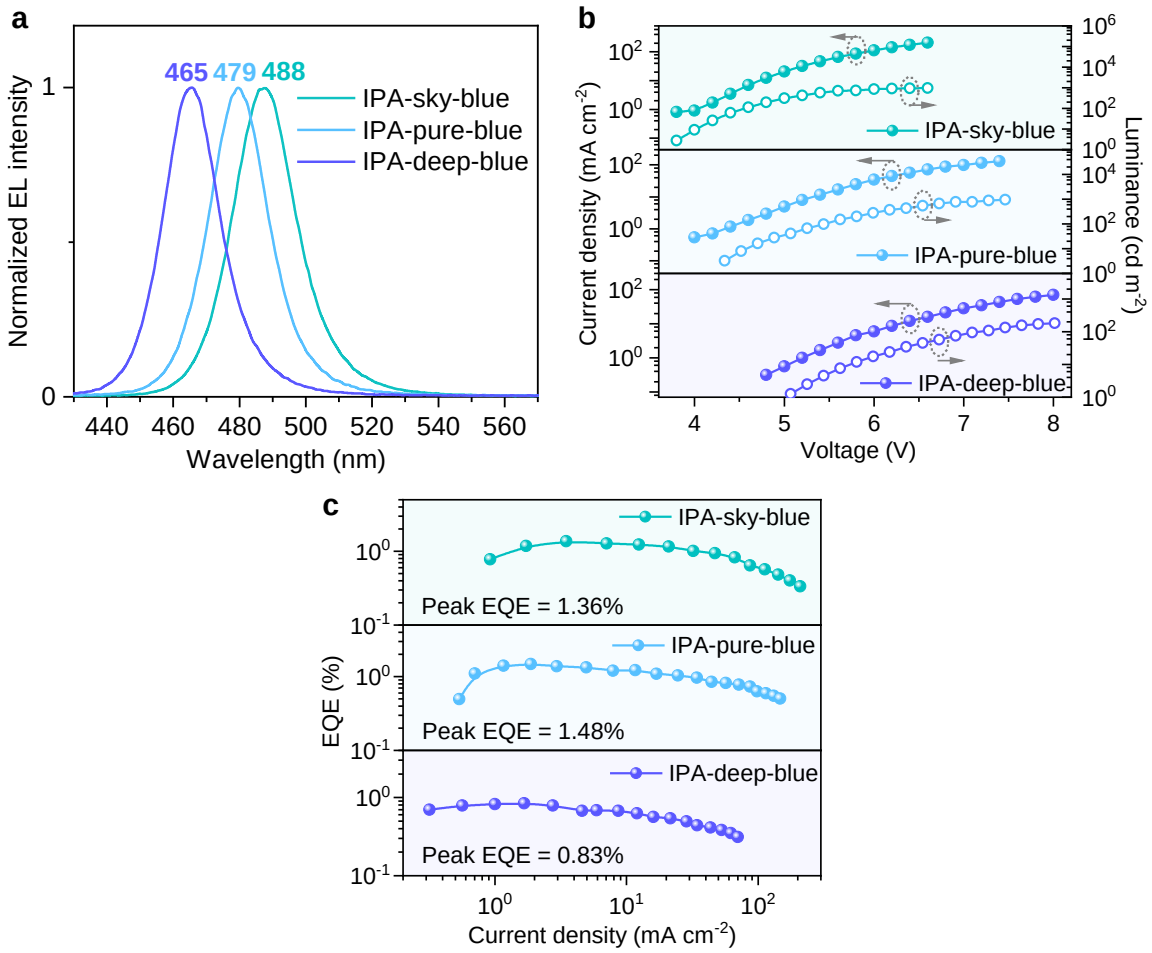

Supplementary Fig. 24. Performance of IPA post-treated devices. a Normalized EL spectra. **b** *J-V-L* characteristic curves. **c** Dependence of the EQE versus current density.

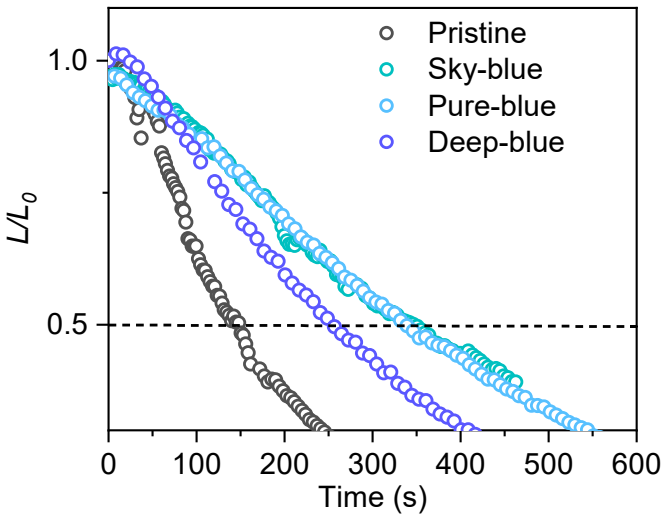

Supplementary Fig. 25. Characterization of device stability. Operational lifetimes of the pristine and CF post-treated devices tested at a constant J of 1 mA cm^{-2}.

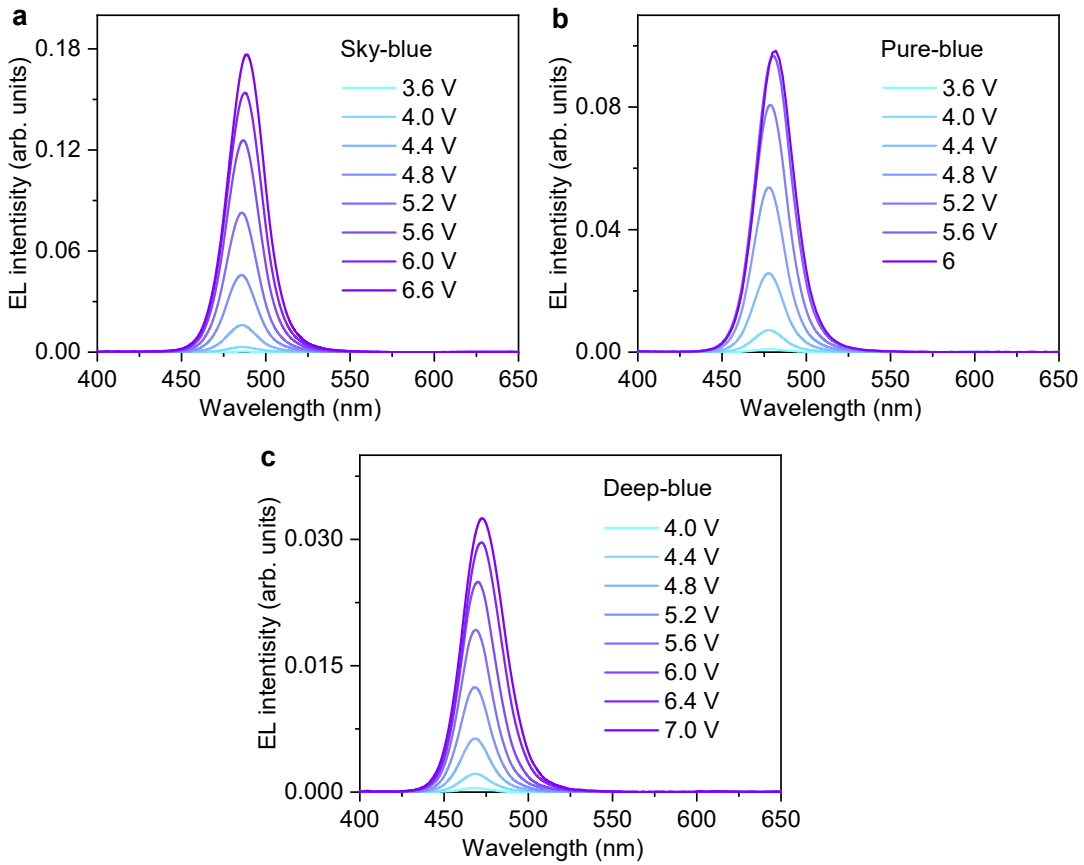

Supplementary Fig. 26. EL spectral stability of CF post-treated devices. EL spectra of the (**a**) sky-, (**b**) pure-, and (**c**) deep-blue devices with CF post-treatment under various driving voltages.

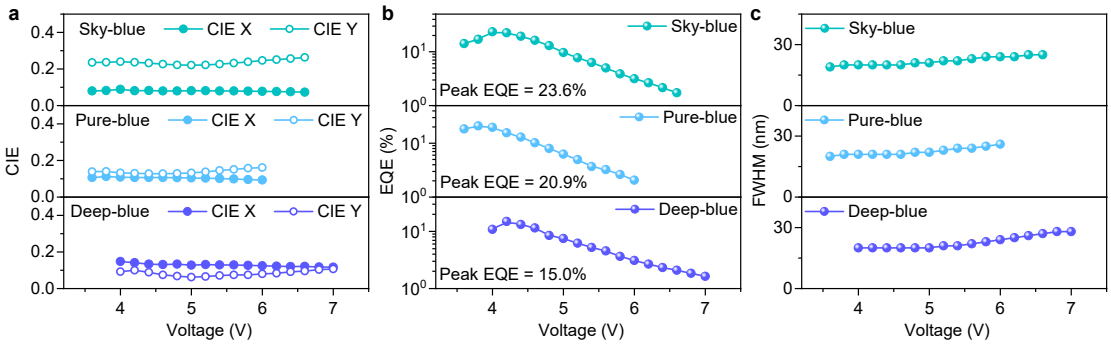

Supplementary Fig. 27. Performance of CF post-treated devices. **a** Dependence of the CIE coordinates versus voltage. **b** Dependence of the EQE versus voltage. **c** Dependence of the FWHM versus voltage.

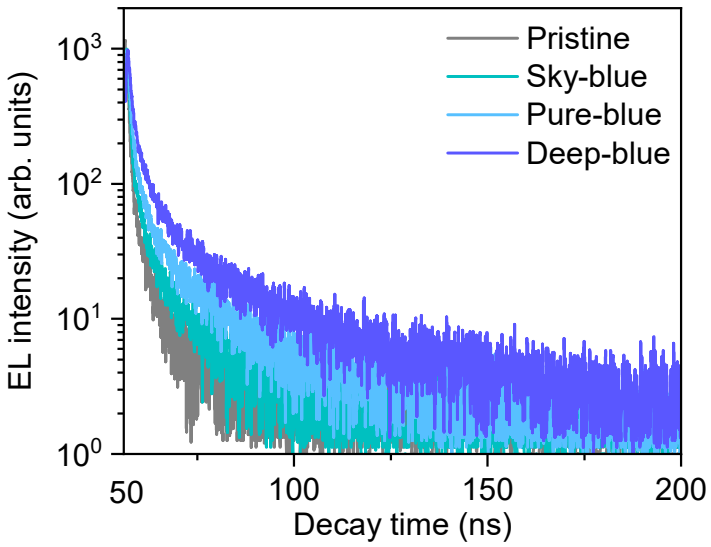

Supplementary Fig. 28. Transient exciton dynamics in devices. Transient electroluminescence decay curves of the pristine and CF post-treated devices.

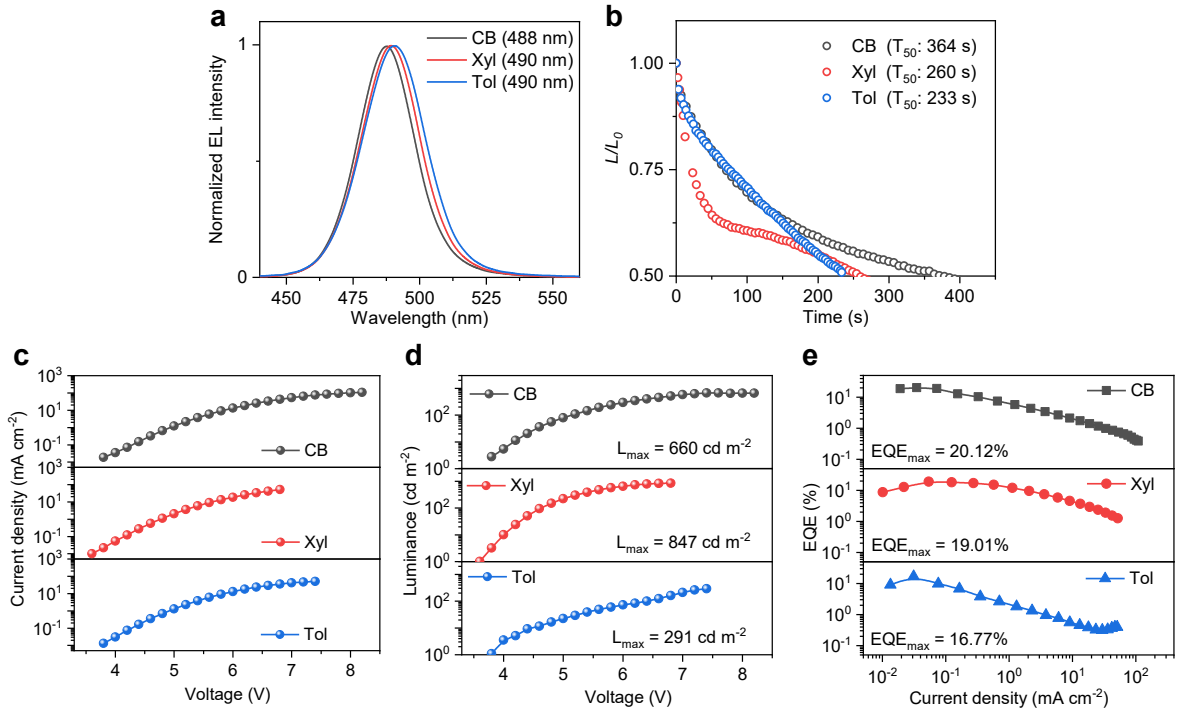

Supplementary Fig. 29. Performance of anti-solvent post-treated devices. a Normalized EL spectra. **b** Dependence of the EQE versus current density. **c** *L*-*V* characteristic curves. **d** *J*-*V* characteristic curves. **e** Operational lifetime curves.

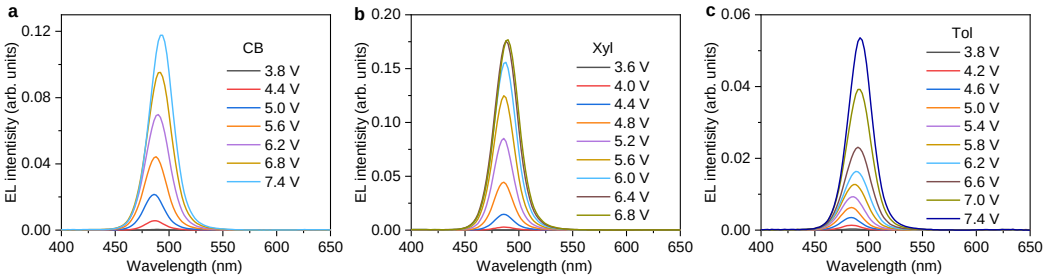

Supplementary Fig. 30. EL spectral stability of anti-solvent post-treated devices. EL spectra with (**a**) CB, (**b**) Xyl, and (**c**) Tol post-treatment under various driving voltages.

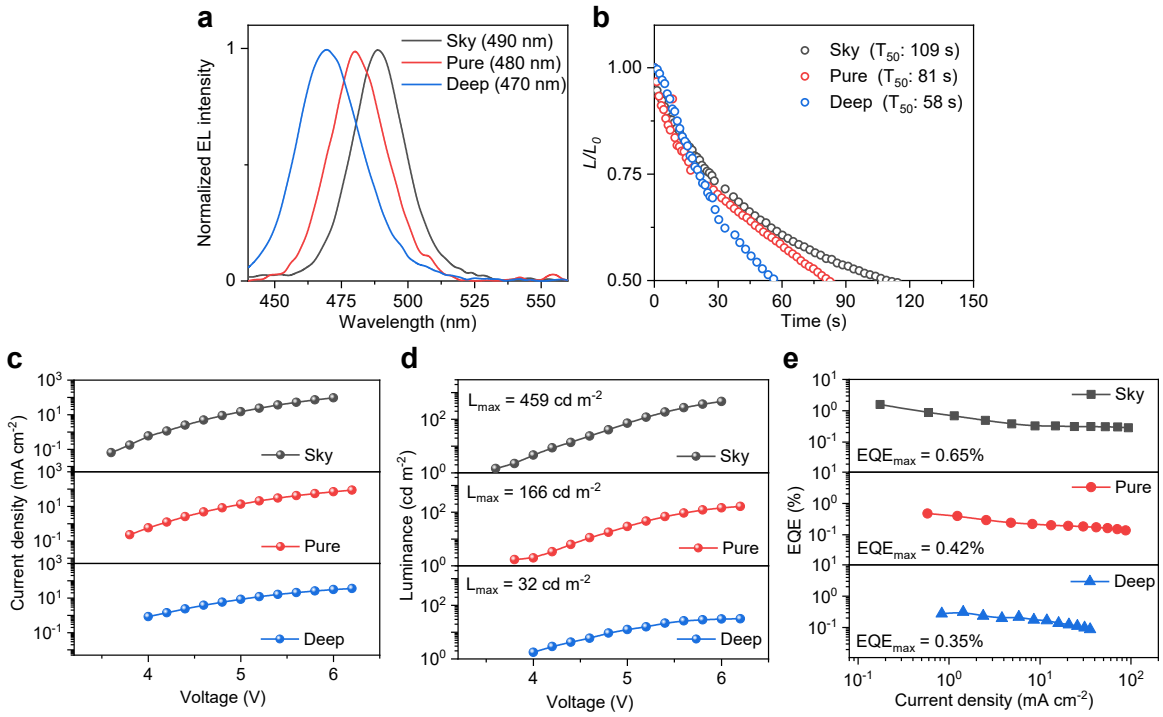

Supplementary Fig. 31. Performance of EtOH post-treated devices. **a** Normalized EL spectra. **b** Dependence of the EQE versus current density. **c** *L*-*V* characteristic curves. **d** *J*-*V* characteristic curves. **e** Operational lifetime curves.

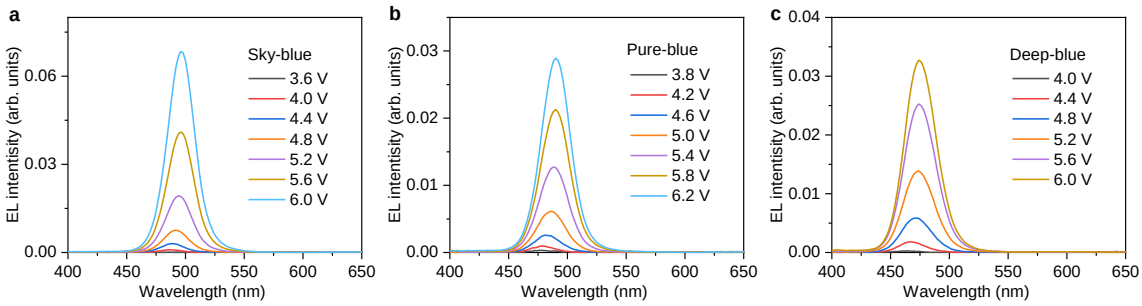

Supplementary Fig. 32. EL spectral stability of EtOH post-treated devices. EL spectra of the (**a**) sky-, (**b**) pure-, and (**c**) deep-blue devices with EtOH post-treatment under various driving voltages.

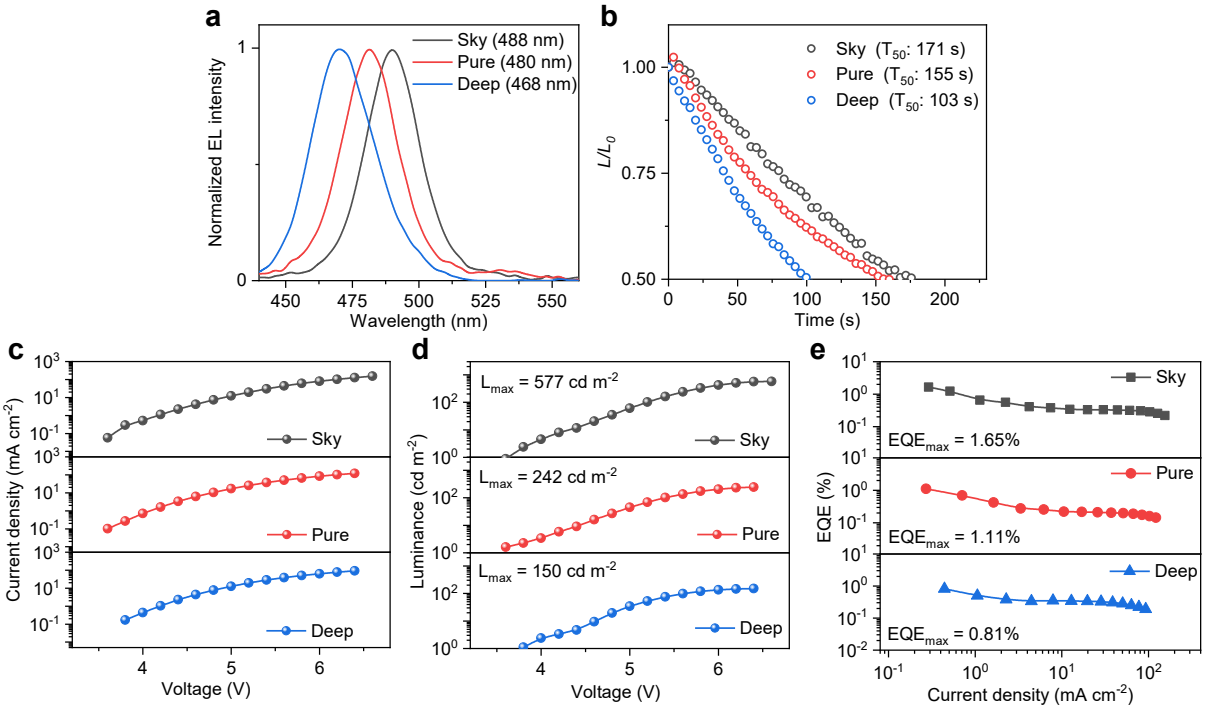

Supplementary Fig. 33. Performance of BuOH post-treated devices. a Normalized EL spectra. **b** Dependence of the EQE versus current density. **c** *L*-*V* characteristic curves. **d** *J*-*V* characteristic curves. **e** Operational lifetime curves.

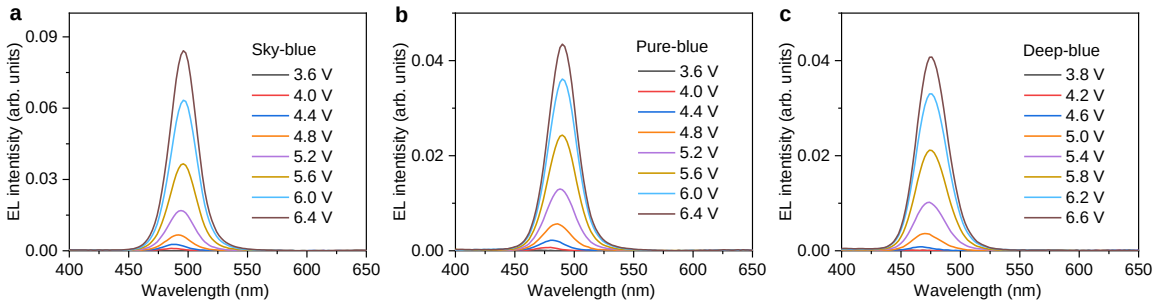

Supplementary Fig. 34. EL spectral stability of BuOH post-treated devices. EL spectra of the (**a**) sky-, (**b**) pure-, and (**c**) deep-blue devices with BuOH post-treatment under various driving voltages.

Supplementary Table 1. Time-resolved PL decay fittings for different perovskite films.

Sample	τ_1 (ns)	A_1	τ_2 (ns)	A_2	τ_3 (ns)	A_3	τ_{avg} (ns)
Pristine	0.82	4101.31	6.38	831.61	50.84	101.26	21.58
Pure CF	1.01	5410.23	7.31	684.61	52.40	90.49	19.08
Pure IPA	0.44	4532.60	3.14	809.55	25.94	76.96	9.27
Sky-blue	2.38	3808.93	11.75	1034.60	77.94	143.64	31.99
Pure-blue	2.20	3834.21	10.03	1136.54	67.89	152.45	27.68
Deep-blue	2.20	3897.26	11.16	1113.01	73.42	143.04	29.48

The sky-, pure-, and deep-blue samples in the table refer to the CF-based post-treated perovskite films. The time-resolved PL curves of control and target perovskite films were fitted using a three exponential decay function of $I(t) = A_1 \times \exp[-t/\tau_1] + A_2 \times \exp[-t/\tau_2] + A_3 \times \exp[-t/\tau_3]$. Here, A_1, A_2 and A_3 are the decay amplitudes of the curve fitting. τ_1, τ_2 and τ_3 correspond to the decay time constants. The average lifetime τ_{avg} was calculated by the relation of $\tau_{avg} = (A_1\tau_1^2 + A_2\tau_2^2 + A_3\tau_3^2) / (A_1\tau_1 + A_2\tau_2 + A_3\tau_3)$.

Supplementary Table 2. Halogen ratios in the sky-, pure-, and deep-blue perovskite films obtained from the XPS measurements.

	Area (Br)	n_{Br}	Area (Cl)	n_{Cl}	$n_{Br/Cl}$
Sky-blue	6432	2264	1483	649	0.77/0.23
Pure-blue	4206	1481	1554	680	0.68/0.32
Deep-blue	6108	2150	3894	1704	0.55/0.45

Supplementary Note 1. Extraction of recombination rate constants

The PLQY values of the pristine, sky, pure and deep blue perovskite films are 42.6%, 72.8%, 56.1% and 48.0% respectively. The average life ($\tau_{average}$) values of the pristine, sky, pure and deep blue perovskite films are 21.58 ns, 31.99 ns, 27.68 ns and 29.48 ns, respectively.

The average life is determined by the radiative and non-radiative recombination rate constants (k_r and k_{nr}):

$$\tau_{average} = (k_r + k_{nr})^{-1} \quad (1)$$

Substitute $\tau_{average}$ into the following formula, we can get the non-radiative recombination rate constants (k_r):

$$PLQY = k_r / (k_r + k_{nr}) \quad (2)$$

Finally, the non-radiative recombination rate constants (k_{nr}) is obtained by substituting k_r into equation of $\tau_{average} = (k_r + k_{nr})^{-1}$. The unit of k_r and k_{nr} is s^{-1}. Two constants can be used to quantitatively characterize the inhibition of additive treatment on the non-radiative recombination process of perovskite films.

Supplementary Note 2. Extraction of exciton binding energy

Perovskite materials generally undergo slight structural phase transition with decreasing temperature. However, this aspect does not affect the dielectric confinement problem. The exciton binding energy of the pristine and target perovskite has been extracted through the fitting procedure.

The exciton binding energy was fitted by Equation as follows:

$$I\ (T) = \frac{I_0}{1+Ae^{(-\frac{E_b}{k_B T})}} \quad (3)$$

where $I\ (T)$ is the temperature-dependent integrated PL intensity, T is the temperature, I_0 is the integrated PL intensity extrapolated at 0 K, A is a constant, E_b is the exciton binding energy and k_B is the Boltzmann constant.

Supplementary References

[1] J. Li, X.Wang, Y. Tan, D. Liang, Y. Zou, L. Cai, T.Wu, K.Wen, Y.Wang, Y. Li, *Adv. Opt. Mater.* **2020**, 8, 2001073.

[2] Y. Shen, J. K.Wang, Y. Q. Li, K. C. Shen, Z. H. Su, L. Chen, M. L. Guo, X. Y. Cai, F. M. Xie, X. Y. Qian, *Adv. Sci.* **2021**, 8, 2102213.

[3] F. Yuan, C. Ran, L. Zhang, H. Dong, B. Jiao, X. Hou, J. Li, Z.Wu, *ACS Energy Lett.* **2020**, 5, 1062.

[4] K. Zhang, Z. Su, Y. Shen, L. Cao, X. Zeng, S. Feng, Y. Yu, X. Gao, J. Tang, and Y. Li, *ACS Nano* **2024,** 18 (5), 4570-4578.

[5] M. Karlsson, Z. Yi, S. Reichert, X. Luo, W. Lin, Z. Zhang, C. Bao, R. Zhang, S. Bai, G. Zheng, P. Teng, L. Duan, Y. Lu, K. Zheng, T. Pullerits, C. Deibel, W. Xu, R. Friend, F. Gao, *Nat. Commun.* **2021**,12, 361.

[6] Z. Ren, J. Sun, J. Yu, X. Xiao, Z. Wang, R. Zhang, K. Wang, R. Chen, Y. Chen, W. C. H. Choy, *Nanomicro Lett.* **2022**, 14, 66.

[7] S. Liu, Z. Guo, X. Wu, X. Liu, Z. Huang, L. Li, J. Zhang, H. Zhou, L. D. Sun, C. H. Yan, *Adv. Mater.* **202**3, 35, 2208078.

[8] S. Yuan, L. S. Cui, L. Dai, Y. Liu, Q. W. Liu, Y. Q. Sun, F. Auras, M. Anaya, X. Zheng, E. Ruggeri, Y. J. Yu, Y. K. Qu, M. Abdi-Jalebi, O. M. Bakr, Z. K. Wang, S. D. Stranks, N. C. Greenham, L. S. Liao, R. H. Friend, *Adv. Mater.* **2021**, *33*, 2103640.

[9] Z. Chu, W. Zhang, J. Jiang, Z. Qu, F. Ma, Y. Zhao, X. Chu, Y. Shen, Y. Li, Z. Yin, X. Zhang, J. You, *Nat. Electron.* **2023**, *6*, 360.

[10] S. Yuan, R.-Z. An, L. Dai, Y. Liu, S.-C. Dong, *Nat. Photon.* **2024**. https://doi.org/10.1038/s41566-024-01382-6.

[11] Y. Jiang, C. Sun, J. Xu, S. Li, M. Cui, X. Fu, Y. Liu, Y. Liu, H. Wan, K. Wei, T. Zhou, W. Zhang, Y. Yang, J. Yang, C. Qin, S. Gao, J. Pan, Y. Liu, S. Hoogland, E. H. Sargent, J. Chen, M. Yuan, *Nature* **2022**, 612, 679.

[12] Z. Li, Z. Chen, Y. Yang,Q. Xue,H.-L. Yip, Y. Cao, *Nat. Commun.* **2019**, 10, 1027.

[13] Y. Yu, B. F. Wang, Y. Shen, Z. H. Su, K. Zhang, H. Ren, Y. Q. Li, *Angew. Chem.* **2024**, 136(7), e202319730.

[14] M. Worku, A. Ben-Akacha, S. Sridhar, J. R. Frick, S. Yin, Q. He, A. J. Robb, M. Chaaban, H. Liu, J. R. V. Winfred, Adv. Funct. Mater. **2021**, 31, 2103299.

[15] Y. Yang, S. Xu, Z. Ni, C. H. Van Brackle, L. Zhao, X. Xiao, X. Dai, J. Huang, *Adv. Mater.* **2021**, *33*, 2100783.

[16] Y. Liu, S. Wang, Z. Yu, G. Chen, C. Wang, T. Wang, W. Ke, G. Fang, *Adv. Mater.* **2023**, 35, 2302161.

[17] S. Yuan, Z. K. Wang, L. X. Xiao, C. F. Zhang, S. Y. Yang, B. B. Chen, H. T. Ge, Q. S. Tian, Y. Jin, L. S. Liao, *Adv. Mater.* **2019**, 31, 1904319.

[18] Y. Nong, J. Yao, J. Li, L. Xu, Z. Yang, C. Li, J. Song, *Adv. Mater.* **2024**, 2402325.

[19] Y. Liu, Z. Li, J. Xu, Y. Dong, B. Chen, S. M. Park, D. Ma, S. Lee, J. E. Huang, S. Teale, O. Voznyy, E. H. Sargent, *J. Am. Chem. Soc.* **2022**, 144, 4009

[20] L. Ma, X. Li, X. Chen, J. Li, P. Liu, C. Wei, Q. Ma, L. Xu, W. Zhang, J. Song, *Chem. Eng. J.* **2023**, 474, 145732.

[21] Y. Dong, Y. K. Wang, F. Yuan, A. Johnston, Y. Liu, D. Ma, M. J. Choi, B. Chen, M. Chekini, S. W. Baek, L. K. Sagar, J. Fan, Y. Hou, M. Wu, S. Lee, B. Sun, S. Hoogland, R. Quintero-Bermudez, H. Ebe, P. Todorovic, F. Dinic, P. Li, H. T. Kung, M. I. Saidaminov, E. Kumacheva, E. Spiecker, L. S. Liao, O. Voznyy, Z. H. Lu, E. H. Sargent, *Nat. Nanotechnol.* **2020**, 15, 668.

[22] J. Luo, L. Yang, Z. Tan, W. Xie, Q. Sun, J. Li, P. Du, Q. Xiao, L. Wang, X. Zhao, *Adv. Mater.* **2021**, 33, 2101903.

[23] A. Liu, C. Bi, J. Li, M. Zhang, C. Cheng, D. Binks, J. Tian, Nano Lett. 2023, 6, 2405.

[24] Y.-K. Wang, F. Jia, X. Li, S. Teale, *Sci. Adv.* **2023**, 9, 2140.

[25] Y. Jiang, K. Wei, C. Sun, Y. Feng, L. Zhang, M. Cui, S. Li, W. D. Li, J. T. Kim, C. Qin, M. Yuan, *Adv. Mater.* **2023**, 35, 2304094.